Cytoskeleton

WILEY

CYTOSKELETON

RESEARCH ARTICLE OPEN ACCESS

PEK14: A Kinesin-4 Necessary for Male-Derived Fertility in *Arabidopsis thaliana*

Isabella N. Mendes | Norman R. Groves | Jessica Z. Li | Lily N. Thompson | Brian J. Smith | Aman Y. Husbands | Iris Meier

Department of Molecular Genetics, The Ohio State University, Columbus, Ohio, USA

Correspondence: Iris Meier (meier.56@osu.edu)

Received: 17 February 2025 | **Revised:** 9 May 2025 | **Accepted:** 15 May 2025

Funding: This work was supported by National Science Foundation (NSF-2023348) to IM.

Keywords: *Arabidopsis thaliana* | kinesin-4 | male germ unit | phragmoplast | pollen tube

ABSTRACT

Of the 61 kinesins annotated in *Arabidopsis thaliana*, many are still without assigned function. Here, we have screened an insertional mutant library of Arabidopsis pollen-expressed kinesins for fertility defects. Insertional mutants for three kinesins showed a significant reduction in seed set. Among them, we focused on the sole kinesin-4 expressed in pollen (kinesin-4C, here Pollen-Expressed Kinesin 14, PEK14). We show a seed-set defect in the three independent alleles *pek14-1, pek14-2, and pek14-3*. This defect is male-derived and is equally distributed throughout the silique. Mature *pek14-1* anthers contain about 10% inviable pollen grains. *pek14-1* pollen tubes grow 20% more slowly and show reduced pollen tube bending. Analysis of the male germ unit (MGU), as it travels through the pollen tube, demonstrates an aberrant organization of the *pek14-1* MGU in 30% of pollen tubes and an increase in the distance of the MGU to the tip by 24%. Expression of GFP-tagged PEK14 successfully complemented the observed seed set defect, as well as the growth rate, bending, and MGU organization defects observed in *pek14-1*. In pollen, PEK14-GFP is located diffusely at the pollen tube tip. PEK14-GFP is also expressed in the root meristematic zone and is located at the mid-zone of the phragmoplast, but no apparent root growth phenotype was observed, likely due to redundancy in this organ.

1 | Introduction

Motor proteins are molecular machines that use energy from the hydrolysis of ATP to move along the cytoskeleton. They function in a broad range of processes ranging from cell division to vesicle trafficking. Plants possess two types of motor proteins: kinesins, which interact with microtubules (MTs), and myosins, which interact with F-actin (Nebenführ and Dixit 2018). Only two of the 13 classes of myosins are represented in plants, Class VII and XI, encompassing 17 individual myosins (Sellers 2000; Reddy and Day 2001; Lee and Liu 2004; Nebenführ and Dixit 2018). The myosins of the model plant *Arabidopsis thaliana* (Arabidopsis) are well studied, and many of their roles have been identified (Avisar et al. 2009; Sparkes 2011; Wu and Bezanilla 2014; Haraguchi et al. 2018).

Kinesins have been classified into 14 separate classes (Lawrence et al. 2004). Arabidopsis codes for 61 kinesins, which fall into ten classes: Kinesin-1, -4, -5, -6, -7, -8, -10, -12, -13, and -14. In addition, there are three kinesins in Arabidopsis (ARK1, 2, and 3), which do not belong to any class (Figure 1A, Richardson et al. 2006; Zhu and Dixit 2012). The Kinesin-7 and Kinesin-14 classes are particularly well represented, with fifteen Kinesin-7s and twenty-one Kinesin-14s. The expansion of kinesin gene families in plants might be related to the absence of dyneins (Gicking et al. 2018). Thus, in plants, minus-end directed kinesins might take on the role of animal and fungal dynein (Yamada et al. 2017).

While many animal and fungal kinesins have been investigated at the cellular and molecular level, kinesins in plants remain

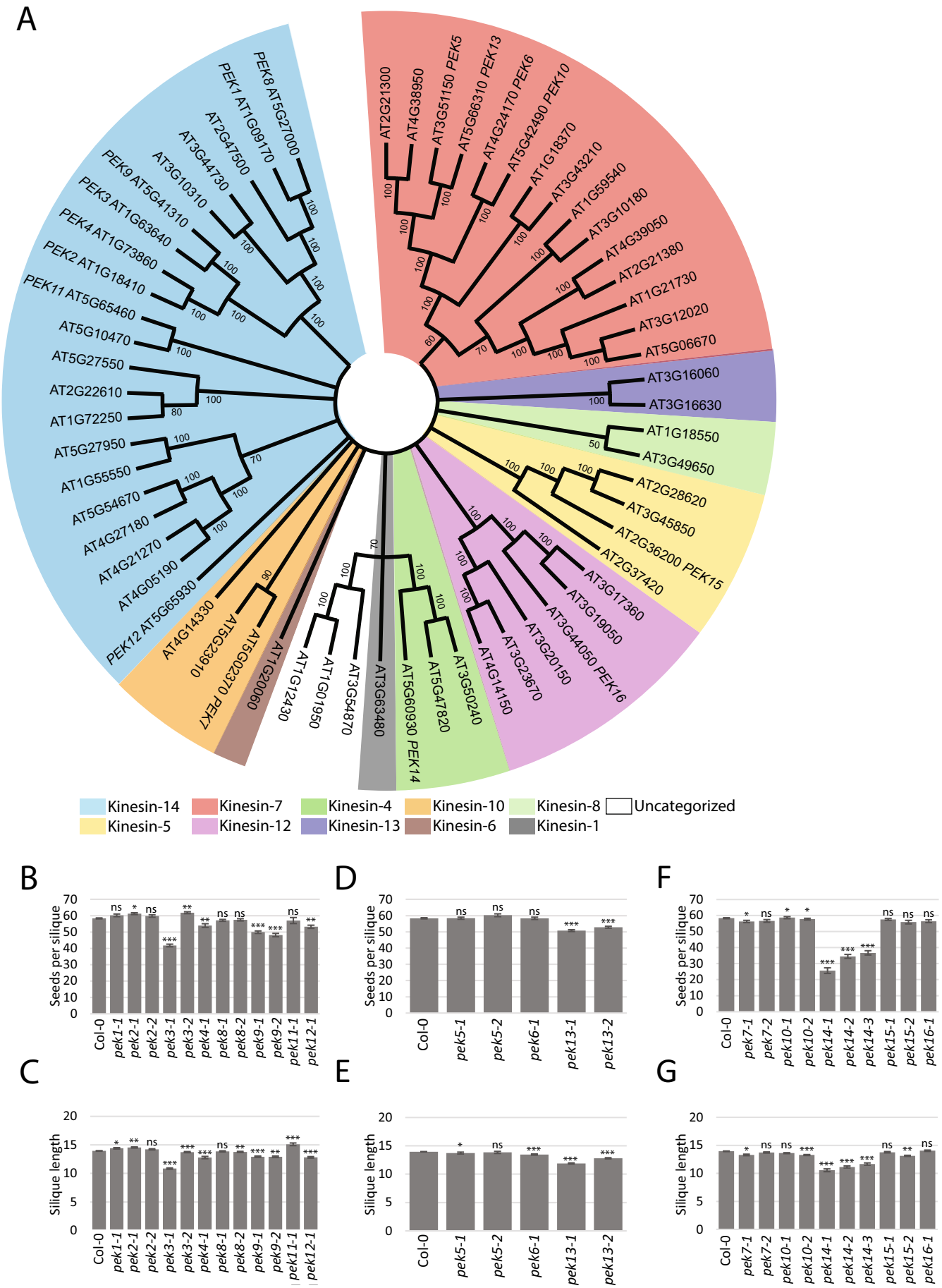

FIGURE 1 | Legend on next page.

FIGURE 1 | Identification of pollen-expressed kinesins involved in fertility. (A) Phylogenetic tree of Arabidopsis kinesins, with the Pollen-Expressed Kinesins (PEK) investigated here indicated. Colors indicate kinesin subfamilies, as indicated in the key. Numbers in the phylogenetic tree indicate boot-strap values. (B–G) Seed set (B, D, F) and silique length (C, E, G) measurements of *pek* mutants. Mutant lines (Table S2) are grouped by class: Kinesin-14s (B, C), Kinesin-7s (D, E), and remaining kinesin classes (F, G). $N > 100$ siliques analyzed for each genotype. Statistics are compared to Col-0 control and calculated using Student's *t*-test: $P < 0.05 = *$, $p < 0.005 = **$, $p < 0.0005 = ***$. Error bars show standard error (Table S3).

an area of emerging research (Zhu and Dixit 2012). Several kinesins have been assigned roles in cell division and mitosis. A pair of phragmoplast-orienting Kinesin-12s (POK1 and POK2) in *Arabidopsis* is involved in the establishment of the cortical division zone (Lipka et al. 2014). Several kinesins are involved in the assembly, maintenance, and cellular positioning of the spindle apparatus, such as AtKRP125b (PEK15), a Kinesin-5 (Strauß et al. 2021), KINESIN-12E (PEK16), a Kinesin-12 (Herrmann et al. 2021), and ATK1 and ATK5, two highly similar Kinesin-14s (Hotta et al. 2022). Other kinesins have roles in reproduction, such as MDKIN2, an *Arabidopsis* Kinesin-2 which plays roles in pollen and seed development (Galindo-Trigo et al. 2020), and Calponin homology domain-containing Kinesin-14s, which have been proposed to play a role in the trafficking of sperm cells through the pollen tube (Schattner et al. 2021). The latter have also been shown to interact with actin and are involved in pre-mitotic nuclear migration (Preuss et al. 2004; Frey et al. 2010). The wealth of these rather recent discoveries suggests that investigating the currently uncharacterized plant kinesins might be fruitful to connect them to additional biologically relevant processes (Lee and Liu 2004; Nebenführ and Dixit 2018).

The Kinesin-4 family is further broken down into five subfamilies: KIF4, KIF7, KIF21, NcKIF21A, and KIF27. The KIF4 subfamily is named for the mammalian KIF4 gene, which was first discovered in 1992, when it was shown to be involved in transport within mice neuronal cells (Aizawa et al. 1992). Shortly thereafter, it was identified as a chromatin interactor during mitosis (Wang and Adler 1995). Humans have two KIF4 subfamily members, *KIF4* and *KIF4B*, that are likely functionally redundant (Miki et al. 2001). KIF4 is the only Kinesin-4 subfamily present in *Arabidopsis*, where it accounts for the three *Arabidopsis* Kinesin-4 members *At*KN4A (KINESIN-4A, FRA1), *At*KN4B (KINESIN-4B), and *At*KN4C (KINESIN-4C, PEK14) (Richardson et al. 2006; Kong et al. 2015; Zhu et al. 2015; Yue et al. 2018). FRA1 (FRAGILE FIBER 1) and KINESIN-4B are more closely related to each other than to PEK14 (Kong et al. 2015; Zhu et al. 2015). Only FRA1 has been studied in detail.

Human KIF4, together with the microtubule-bundling protein PRC1, plays an essential role in the spindle midzone/midbody organization in vertebrate cytokinesis (Kurasawa et al. 2004; Zhu and Jiang 2005). In vitro experiments with Xenopus homologs showed that KIF4 and PRC1 are sufficient to shorten the MT overlap region, with KIF4 being recruited to the antiparallel MT region by autonomously binding PRC1 (Bieling et al. 2010).

In Arabidopsis, FRA1 was first identified as a factor in secondary cell wall deposition. In a *fra1* mutant, the mechanical strength of fibers in the inflorescence stem of Arabidopsis was dramatically reduced. While this was originally considered a defect in cellulose microfibril orientation (Zhong et al. 2002), this hypothesis could later not be confirmed (Zhu et al. 2015). FRA1 is associated with vesicles most likely involved in the transport of non-cellulosic cell-wall material along cortical microtubules (Kong et al. 2015; Zhu et al. 2015). In addition, FRA1 stabilizes cortical microtubules and binds to cellulose-synthase-microtubule uncoupling protein (Ganguly et al. 2020). Disruption of FRA1 resulted in several defects in growth and development. Mutant plants were stunted due to a lack of cell elongation and axial growth. This stunting indirectly impacted fertility, resulting in shorter siliques filled with fewer seeds (Kong et al. 2015). Interestingly, double mutants of *fra1* and *kinesin-4c* (*pek14-1*) resulted in a more severe phenotype across all these defects, including a dramatic reduction in the number of seeds per silique (Kong et al. 2015). To our knowledge, this finding is the only currently published data examining *At*KN4C/PEK14.

While one of the earliest pieces of evidence for the existence of kinesins in plants stemmed from work on pollen tubes (Tiezzi et al. 1992), the role of MTs and kinesins in pollen tubes has thereafter been long debated (Romagnoli et al. 2001; Cai and Cresti 2010; Chebli et al. 2013; Cai 2022). While there is a considerable amount of knowledge on the role of actin and myosins, it is still rather unclear what role MTs, and by extension kinesins, play in the transport of organelles and vesicles in conjunction with pollen tube elongation, change of growth direction, cell-wall composition, and sperm cell delivery.

Here, a targeted screen was performed in Arabidopsis with the goal to identify kinesin mutants that negatively affect male fertility. Homozygous insertional mutants for 16 pollen-expressed kinesins (PEKs) were tested for seed set defects. Insertional mutants of three kinesins displayed a significant reduction in seed set. The most severe defect was observed when mutating *AtKN4C* (*PEK14*). We demonstrate here that PEK14 is located at the tip of elongating pollen tubes. Lack of PEK14 results in small but significant defects in pollen tube elongation, pollen tube tip flexibility, MGU movement, and MGU positioning. Taken together, these phenotypes—possibly additive to still unknown effects—likely contribute to the observed seed-set defect and demonstrate a formerly unknown role for a plant kinesin in MGU transport and pollen tube tip organization. In addition, PEK14 is associated with the cell-plate-adjacent side of the phragmoplast throughout root cell division.

2 | Material and Methods

2.1 | Selection of Pollen-Expressed Kinesins

To identify Arabidopsis kinesins highly or preferentially expressed in pollen, we utilized the list of 61 putative Arabidopsis kinesins previously reported (Lee and Liu 2004; Zhu et al. 2015). The Arabidopsis kinesin evolutionary history was inferred by

using the Maximum Likelihood method and JTT matrix-based model (Jones et al. 1992). Initial tree(s) for the heuristic search were obtained automatically by applying Neighbor-Joining and BioNJ algorithms to a matrix of pairwise distances estimated using the JTT model and then selecting the topology with superior log likelihood value. Evolutionary analyses were conducted in MEGA11 (Tamura et al. 2021). Expression data for each kinesin were visualized using the Arabidopsis eFP browser (https://bar.utoronto.ca/efp2/) (Winter et al. 2007). The "Developmental Map" source data were used, a snapshot of gene expression in a variety of tissues over the course of development. For each individual gene, the relative expression level was color-coded in each tissue and stage, with red indicating the 80th percentile and yellow indicating the 40th percentile or lower. The expression values of the program output for each gene were compared between mature pollen and all other samples. Kinesins were deemed to be enriched in pollen if expression was in the 80th percentile or higher in pollen and/or stage 15 flowers and in the 40th percentile or lower in the remaining developmental tissues. The kinesins that fit this criterium were named "pollen-expressed kinesins" (PEKs) and numbered from 1 to 13.

An additional screen was conducted using a secondary database for expression data, Arabidopsis Heat Tree Viewer (http://pheattreecit.services.brown.edu/). Through this database, the expression of kinesins in reproductive tissues was compared with the expression in somatic tissues. Similar to above, kinesins that displayed expression in the 80th percentile or above for a reproductive tissue and 40th percentile or below for developmental tissues were selected for further study. PEKs 14–16 were identified using this method (Table S1).

2.2 | Plant Material

Columbia-0 (Col-0) ecotype *Arabidopsis thaliana* wild-type seeds and T-DNA insertion mutant lines were obtained from the Arabidopsis Biological Resource Center (ABRC) (Table S2). PCR utilizing gene-specific primers was performed following protocols appropriate for the corresponding T-DNA insertional mutant (SALK, SAIL, GABI-Kat, or WiscDsLox) to either confirm homozygosity or genotype segregating populations and develop homozygous seed stocks (Table S3) (McElver et al. 2001; Sessions et al. 2002; Alonso et al. 2003). Heterozygous *male sterility-1* (*ms1*) used for semi-in vivo pollen tube growth was also obtained from the ABRC (Wilson et al. 2001; Yang et al. 2007).

Arabidopsis seeds were surface sterilized using 70% (v/v) ethanol, then allowed to dry on autoclaved Whatman 3 MM filter paper. Sterilized seeds were plated on Murashige and Skoog (MS) medium plates (Caisson Laboratories) containing 1% sucrose and were vernalized in the dark at 4°C for 48 h before transfer to a 21°C growth chamber under constant light. Seedlings were grown on plates until the four-leaf stage (approximately 10 days after vernalization) and then transplanted to soil where they were grown under 16 h light / 8 h darkness conditions.

2.3 | Seed Set and Silique Length Measurements

Plants were grown in 4″ pots until maturity, with one *pek* mutant per flat. Wild type Col-0 plants were either grown in the same flat or alongside experimental flats. Plants were grown until siliques began to yellow. Yellowed siliques were collected prior to senescence and cleared using 70% ethanol, with at least 100 siliques collected for each genetic background. Silique images were taken using a Nikon SMZ1270 stereo microscope with 3.15x magnification. Data analysis was performed in Fiji (https://fiji.sc/), where the length of each silique was measured and the number of seeds was counted (Schindelin et al. 2012). To determine statistical significance, Student's *t*-test was utilized.

2.4 | Reciprocal Crosses

Reciprocal crosses were performed between Arabidopsis wild type (WT; Col-0 ecotype) plants and *pek14-1* (SALK_124215). As a control, Col-0 pollen was used to pollinate Col-0 flowers. Three experimental crosses were performed, with *pek14-1* pollen used to pollinate Col-0 flowers, Col-0 pollen being used to pollinate *pek14-1* flowers, and *pek14-1* pollen being used to pollinate *pek14-1* flowers. Plants were monitored as siliques developed, and when siliques turned yellow, they were removed from crossed flowers and cleared in 70% ethanol at room temperature for two weeks. Silique images were taken using a Nikon SMZ1270 stereo microscope with a 3.15x magnification. Data analysis was performed in Fiji (https://fiji.sc/). The number of seeds in each silique were counted.

Siliques for quadrant analysis were cleared and imaged as described above. The length of each silique was taken by measuring from the stigma-end of a valve to the pedicel-end of the same valve and was divided by four to give four equal length quadrants per silique. The number of seeds per quadrant was counted. If a seed rested at the division line between quadrants, it was included in the count of the quadrant that contained most of its surface area.

2.5 | Ovary Dissection and Ovule Counting

Stage 15 flowers (Alvarez-Buylla et al. 2010) were removed from the plant, and sepals, petals, and anthers were removed. A dissection needle was used to dissect the female tissue. Ovules were removed one at a time from the ovary using a dissecting pin and counted using a Fisherbrand hand tally counter.

2.6 | Dual Viability Staining of Mature Pollen Grains

Pollen viability was quantified using a fluorescein diacetate (FDA, Sigma-Aldrich) and propidium iodide (PI, Sigma-Aldrich) dual viability stain (Hamilton et al. 2015). Briefly, the PI/FDA stain was created by adding 1 μg/mL FDA and 0.5 μg/mL propidium iodide to pollen germination medium (5 mM KCl, 5 mM $CaCl_2$, 1 mM $Ca(NO_3)_2$, 1 mM $MgSO_4$, 10%

sucrose, 0.01% boric acid, in ddH_2O, pH 7.5). Stage 14 flowers were dissected, and anthers were rubbed against slides to release mature pollen. The PI/FDA stain was added to the slide and incubated at room temperature for 20 min before imaging. Viable pollen grains fluoresced green while inviable pollen grains fluoresced red. Samples were excited at 488 nm and 516 nm, and the detector range was set to 490–470 nm and 566–610 nm, respectively.

2.7 | Aniline Blue Staining of Pistils

Aniline blue staining was performed as described previously (Mori et al. 2006). Briefly, Arabidopsis *ms-1* pistils were pollinated with WT pollen, *pek14-1* pollen, or left unfertilized and allowed to develop for 24 h, at which time they were dissected and placed into a 1.7 mL Eppendorf tube with a 1:3 solution of acetic acid to 100% ethanol. Pistils were fixed in this solution for 2 h at room temperature, then washed in consecutive 70%, 50%, and 30% ethanol washes, followed by a ddH_20 wash. Each wash lasted 10 min. Pistils were transferred to a small petri dish and placed in 8 M NaOH overnight at room temperature. The pistils were then washed with ddH_20 and stained with decolorized aniline blue solution (0.1% w/v aniline blue in 108 mM K_3PO_4 at pH ~11). Pistils were then transferred to slides and imaged using a Nikon Eclipse C90i confocal microscope. Samples were excited at 405 nm and the detector range was set to 410–470 nm.

2.8 | Semi-In Vivo Pollen Tube Growth

Semi-in vivo pollen tube growth was performed essentially as described previously (Zhou and Meier 2014; Dickinson et al. 2018). Briefly, stigmas of *male sterility-1* plants (*ms1*) (Wilson et al. 2001; Yang et al. 2007) were pollinated with experimental pollen and allowed to begin germination (Yang et al. 2007). After 2 h, stigmas were dissected and placed into pollen germination media (5 mM KCl, 5 mM $CaCl_2$, 1 mM $Ca(NO_3)_2$, 1 mM $MgSO_4$, 10% sucrose, 0.01% boric acid, in ddH_2O, pH 7.5) on slides. After 5 h of pollen tube germination (7 h post-pollination), pollen tubes were imaged using a Nikon Eclipse C90i confocal microscope.

2.9 | Pollen Tube Straightness Assay

Pollen tube straightness analysis was performed as previously described (de Keijzer et al. 2023) on images collected from semi-in vivo pollen tubes grown as described above. Image analysis was done using Fiji (https://fiji.sc/). Briefly, the segmented line tool was used to measure a straight line from the pollen tube tip 100 μm back up the pollen tube. Then, a segmented line was used to trace the distance from the identified point to the pollen tube tip, following the curvature of the pollen tube. The ratio between the linear path distance and the curved path distance was used as a measure of straightness, with a value of one indicating a straight pollen tube and values less than one indicating a curved or meandering pollen tube.

2.10 | MGU Order and Distance to Tip Measurements

Semi-in vivo pollen tube growth was performed as described above with the following change: SYBR green (ThermoFisher Scientific, catalog number: S7563) was added to the pollen germination media as a 1:4000 dilution of the 10,000 x concentrate stock, as described previously (Motomura et al. 2021). The pollen tube germination time was reduced from 5 h (7 h post-pollination) to 3 h (5 h post-pollination). Pollen tubes were imaged on a Nikon Eclipse C90i confocal microscope. Images were analyzed using Fiji (https://fiji.sc/).

MGU order was determined by observing sperm cells and the vegetative nucleus within the pollen tube and categorizing the MGU organization into one of seven types: "SC Only", "SC Ahead", "SC Far Ahead", "Overlapped", "VN Only", "VN Far Ahead", and "VN Ahead" – which were categorized as follows. SC Ahead: The sperm cells were ahead of the VN, but not more than two lengths of the VN ahead of the VN. SC Far Ahead: The SCs were more than two VN lengths ahead of the VN. Overlapped: The SCs and VN were alongside one another. VN Only: Only the VN was visible within 100 μm of the pollen tube tip. VN Far Ahead: The VN was more than two lengths of the VN ahead of the SCs. VN Ahead: The VN was ahead of the SCs, but less than two lengths of the VN ahead of the SCs.

To measure the distance to the tip for the MGU components, Fiji (https://fiji.sc/) was used. The segmented line tool was used to trace the path from the leading edge of the vegetative nucleus and the leading sperm cell along the path of the pollen tube growth to the pollen tube tip. The length of this path was measured.

2.11 | Cloning and Plasmid Construction

To clone the *PEK14* coding sequence, anther cDNA was used, due to low *PEK14* expression in other tissue types. To generate anther cDNA, anthers from 12 *Arabidopsis* plants were harvested and used for cDNA synthesis. RNA isolation from the anther tissue was performed either by a Nucleospin RNA Plant Kit (item number 740949.50 from Macherey-Nagel) or by RNA extraction with TRIzol (TRIzol Reagent, catalog number 15596026 from ThermoFisher Scientific); (Shi and Bressan 2006). RNA was then used in RT-PCR to create anther cDNA, using Oligo d(T) primers (Invitrogen SuperScript II First-Strand Synthesis System kit, catalog number 18080051 from ThermoFisher Scientific).

PCR was performed from cDNA using a Phusion High-Fidelity DNA Polymerase kit (Catalog number M0530S from New England Biolabs). Attempts to clone the entire *PEK14* cDNA in one fragment were unsuccessful, so the cDNA was amplified in two fragments: a DNA fragment representing the motor protein without the motor domain (the "delta-motor" portion of the protein; Δmotor portion), and the motor portion including a 50 nucleotide overlap with the Δmotor portion (for primers used see Table S3). They were then combined into a single full-length coding sequence fragment by assembly PCR. The full-length PEK14 coding sequence from assembly PCR was purified using the Monarch DNA Gel Extraction

Kit (catalog number T1020S, New England Biolabs) and recombined into D-Topo, then transformed into *E. coli* (pENTR/D-Topo Cloning Kit, ThermoFisher #K240020).

A region 580 bp upstream from the *PEK14* ATG was selected to represent the promoter region, representing the intergenic region between *PEK14* and At5g60940 (*CSTF50*). Gibson assembly cloning (Gibson Assembly Cloning Kit, catalog number E5510S from New England Biolabs) was used to create a pCR8 vector (obtained from pCR8/GW/TOPO TA Cloning Kit with One Shot TOP10 *E. coli*, catalogue number K250020 from ThermoFisher Scientific) containing C-terminally GFP-tagged versions of full-length *PEK14* under the native *PEK14* promoter ($PEK14_{pro}$::PEK14-GFP). A LR reaction was used to transfer the $PEK14_{pro}$::PEK14-GFP into the pB7GW vector (Gateway LR Clonase II Enzyme mix, catalog number 11791020, ThermoFisher Scientific). Arabidopsis *pek14-1* was transformed with the $PEK14_{pro}$::PEK14-GFP using *Agrobacterium tumefaciens*-mediated floral dip (Clough and Bent 1998).

T_1 seedlings were grown on Murashige and Skoog (Caisson Laboratories) plates containing the antibiotic BASTA at a concentration of 10 μg/mL to select for the T-DNA insertion. T_2 seedlings were grown, bulked, and T_3 progeny were grown on Basta plates again to identify homozygous lines. If all the T_3 progeny from a single T_2 plant grew on the Basta plate, that T_2 lineage was considered homozygous for the T-DNA insertion.

2.12 | Root Imaging and FM4-64 Staining

$PEK14_{pro}$::PEK14-GFP in *pek14-1* was germinated on Murashige and Skoog (Caisson Laboratories) plates, with 1% sucrose, under constant light. 9-day-old seedlings were removed from plates and placed onto slides. A Nikon Eclipse C90i confocal microscope was used to image roots. FM4-64 staining was performed as previously described (Rigal et al. 2015). FM4-64 fluorescence was excited at 488 nm and detected at 699–720 nm.

3 | Results

3.1 | Identification of Pollen-Expressed Kinesins

A list of 61 Arabidopsis putative kinesins, belonging to ten kinesin families, has been previously identified (Figure 1A) (Lee and Liu 2004; Zhu and Dixit 2012). To narrow down kinesins with a possible function in pollen, we reviewed their expression levels during development and across a variety of tissue types from publicly available expression profile browsers (Table S1). 16 kinesins were identified as enriched in pollen and named pollen-expressed kinesins (PEK1-16). They included previously characterized as well as functionally unknown kinesins (Table S2). A total of 6 kinesin classes were identified to include PEKs: Eight Kinesin-14s, one Kinesin-5, one Kinesin-12, one Kinesin-4, one Kinesin-10, and four Kinesin-7s (Figure 1A).

T-DNA insertional mutant alleles from the SALK, SAIL, GABI-Kat, and WiscDsLox mutant collections were obtained from the ABRC. T-DNA insertions in exons near the start of the gene were preferred because they are more likely to be knock-out or severe knock-down alleles. In total, 27 insertional mutant lines were selected, 23 of which were SALK lines (Figure S1 and Table S2).

3.2 | Screening of *PEK* Mutants for Seed Loss

To identify pollen-expressed kinesins potentially involved in male fertility, siliques from each homozygous T-DNA insertion line were analyzed for silique length and number of seeds. The 27 lines were screened in several rounds and always compared to Col-0. Figure 1B–G show the combined results grouped by kinesin classes, with Figure 1B,C, showing kinesin-14s, Figure 1D,E, kinesin-7s and Figure 1F,G, showing all other kinesins.

Several lines showed seed-set reductions, typically accompanied by a reduced silique length. The largest seed set reductions were observed for *pek14-1, pek14-2, pek14-3, pek3-1, pek9-1*, and *pek9-2* (Figure 1B,F). Because disrupting *PEK14* showed the strongest defect, it is one of only three members of the Kinesin-4 clade and the only one expressed in pollen, and because it is represented by three independent T-DNA insertion mutants, we focused on its characterization in this study.

3.3 | Loss of PEK14 Leads to Random Seed Loss Based on a Paternal Effect

Figure S2 shows the position of the T-DNA insertions in the three *PEK14* mutant alleles *pek14-1*, *pek14-2*, and *pek14-3*. RT-PCR was performed on anthers, with primers flanking both the 5′ and 3′ end of the gene, as well as primers flanking the insertion site. In none of the three *PEK14* insertional mutants was a PCR product detected that spanned the insertion site, indicating that no full-length mRNA accumulates in the three *PEK14* mutant lines (Figure S2).

The seed counts were repeated separately for the three *PEK14* mutants, confirming that the seed loss was significant in all three mutants (Figure 2B). The distribution of missing seeds within the silique can provide insight into potential sources of the defect. For example, a preferential loss of seeds near the base of the silique typically indicates an inability of pollen tubes to grow to full length through the carpel. When the number of seeds per quadrant in *pek14-1, pek14-2*, and *pek14-3* was counted, the distribution of seeds among the four quadrants did not differ from Col-0. This suggests that the observed seed loss was not likely caused by a defect in pollen tube elongation (Figure 2C). For further analysis, we chose *pek14-1* as the most 5′ located exon insertion mutation.

To determine if the *PEK14* mutant defect was based on a maternal or paternal effect, reciprocal crosses between *pek14-1* and Col-0 were performed. With Col-0 as the male and *pek14-1* as the female parent, only a slight reduction in seed numbers was observed. With *pek14-1* as the male and either Col-0 or *pek14-1* as the female parent, seed set was severely reduced (Figure 2D). This suggests that the seed set defect is predominantly male-derived. In addition, the number of ovules per ovary in *pek14-1* pistils was counted and did not differ from those of Col-0,

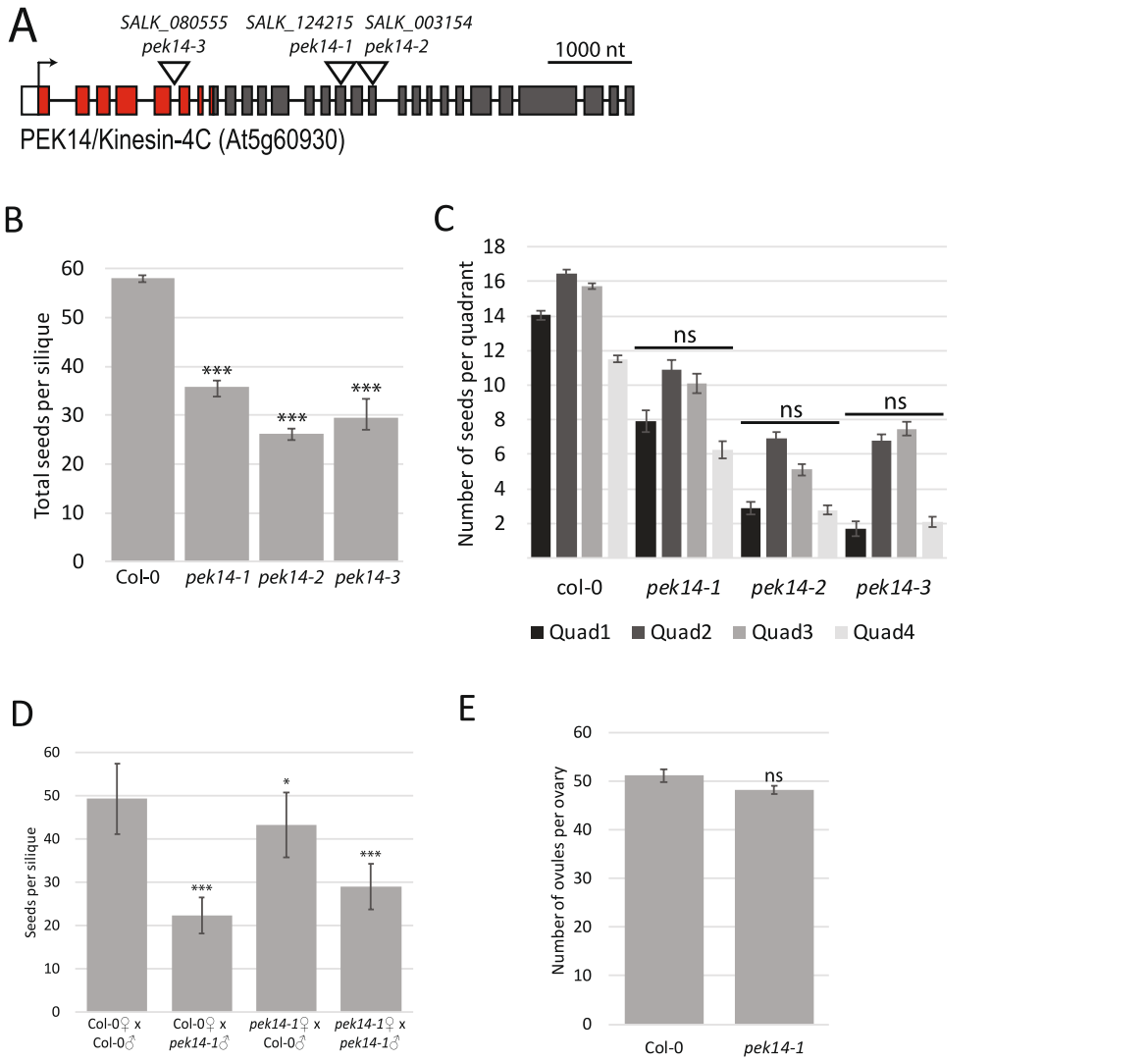

FIGURE 2 | The seed set defect in *pek14* mutants is random and derived from the male parent. (A) Gene diagram showing the position of the three T-DNA insertional mutants in *PEK14*. Red bars indicate exons coding for the motor domain of PEK14. Grey bars indicate exons with non-motor domain coding sequence. White bar, exon containing 5′ UTR. The position of each T-DNA insertion is indicated by triangles above the diagram. (B) Seed set in *pek14* mutant alleles. $N > 100$ siliques per genotype. Statistical significance was determined using Student's *t*-test, in comparison to Col-0. $p < 0.0005 = ***$. Error bars show standard error. (C) Quadrant analysis of PEK14 mutant seed-loss phenotypes. $N > 100$ siliques for all lines. Statistical analysis of distribution of seeds performed with Fisher's exact test, compared to Col-0. Error bars show standard error. (D) Reciprocal crosses of Col-0 and *pek14-1* mutant allele. $N > 30$ siliques for each cross. Statistical significance was determined using Student's *t*-test, in comparison to Col-0. $p < 0.05 = *$, $p < 0.0005 = ***$. Error bars show standard error. (E) Count of ovules per ovary of Col-0 and *pek14-1*. $N > 30$ ovaries for each genotype. Statistical significance compared to Col-0 using Student's *t*-test, $p < 0.05 = *$. Error bars show standard error.

suggesting that defective ovule development is not a cause of the seed loss phenotype (Figure 2E).

3.4 | PEK14 Expression and Localization

The *PEK14* cDNA was cloned and a vector was constructed for expression of a PEK14-GFP-fusion protein under the control of a 580 bp *PEK14* promoter sequence (Figure 3A). C-terminally tagged GFP fusions of other Arabidopsis kinesin-4 proteins have been shown before to be functional (Kong et al. 2015; Zhu et al. 2015; Ganguly et al. 2017). Two transgenic lines—*pek14-1*$^{PEK14\ \#9}$ ($PEK14_{pro}$::PEK14-GFP in *pek14-1* #9) and *pek14-1*$^{PEK14\ \#10}$ ($PEK14_{pro}$::PEK14-GFP in *pek14-1* #10) complemented the *pek14-1* seed-set phenotype to WT levels (Figure 3B).

In addition to being expressed in pollen and anther tissues, *PEK14* mRNA is also expressed in roots (https://bar.utoronto.ca/efp2/) (Winter et al. 2007). When imaging 10-day-old seedling roots, PEK14-GFP expression was primarily detected in the apical meristem, with some minor expression extending into the basal meristem. In both *pek14-1*$^{PEK14\ \#9}$ and *pek14-1*$^{PEK14\ \#10}$, the brightest PEK14-GFP signal was located in a pattern resembling the early cell plate and the edges of the maturing cell plate in cells undergoing division (arrowheads Figure 3C,D) (Lebecq et al. 2022). In non-dividing cells, the PEK14-GFP signal was diffusely distributed in the cytoplasm

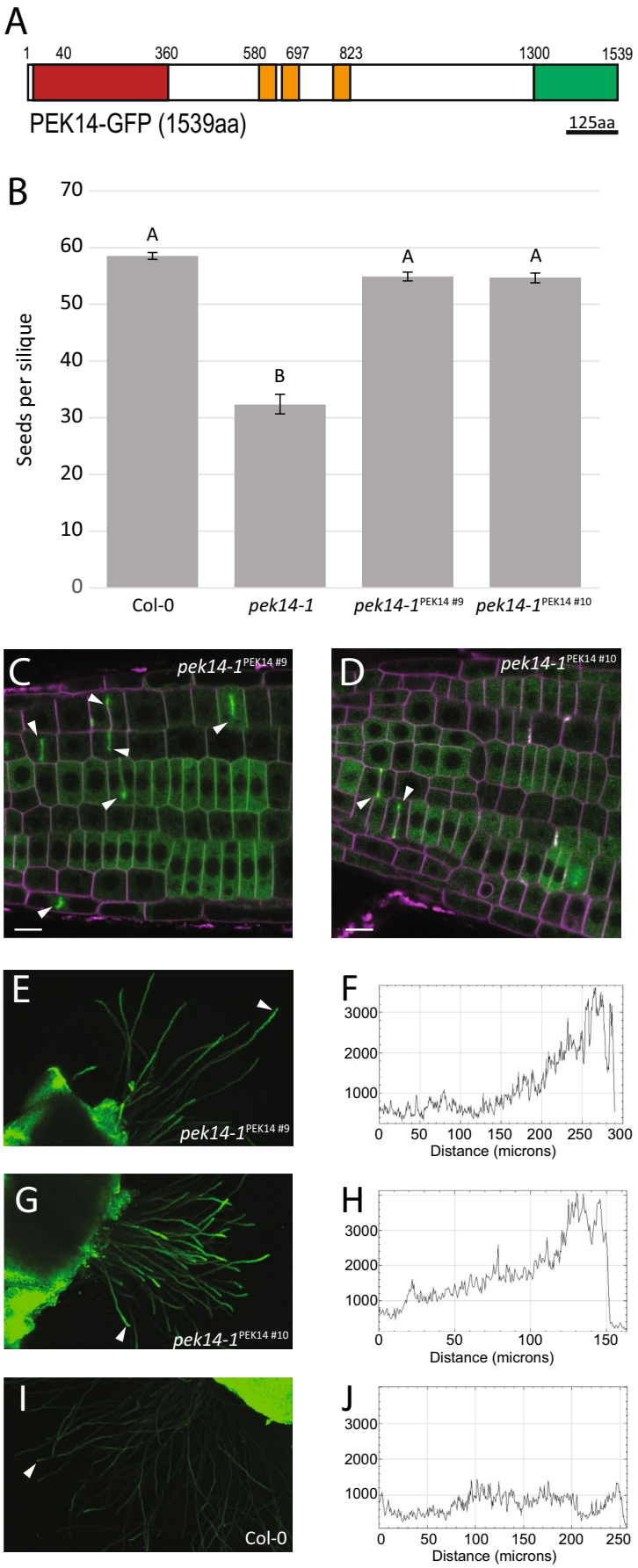

FIGURE 3 | Legend on next page.

FIGURE 3 | PEK14 is diffusely located at the pollen tube tip and associates with the phragmoplast in the seedling root division zone. (A) Domain organization of the PEK14-GFP fusion protein. The motor domain is indicated in red, coiled-coil domains are in orange, and GFP is indicated in green. Numbers above bar indicate amino acid positions. (B) Complementation of the *pek14-1* seed set phenotype by $PEK14_{pro}$::PEK14-GFP in *pek14-1*. The complementation lines *pek14-1*$^{PEK14\ \#9}$ ($PEK14_{pro}$::PEK14-GFP in *pek14-1* #9) and *pek14-1*$^{PEK14\ \#10}$ ($PEK14_{pro}$::PEK14-GFP in *pek14-1* #10) are shown. $N > 100$ siliques for each genotype. Statistical groups were determined using a Tukey–Kramer test following an ANOVA. Error bars show standard error. (C–D) Localization of PEK14-GFP in seedling root tips of *pek14-1*$^{PEK14\ \#9}$ (C), and *pek14-1*$^{PEK14\ \#10}$ (D). Images are single selections taken from a z-stack, with localization at the phragmoplast and cell plate indicated by white arrow heads. Roots were counterstained with FM4-64 (magenta). Scale bar = 10 μm. (E–J) Localization of PEK14-GFP in semi-in vivo germinated pollen tubes. Images of semi-in vivo pollen tubes, 7 h post-pollination, in *pek14-1*$^{PEK14\ \#9}$ (E), *pek14-1*$^{PEK14\ \#10}$ (G), and Col-0 (I). Displayed images are maximum intensity projections. Signal intensity graphs taken along the length of *pek14-1*$^{PEK14\ \#9}$ (F), *pek14-1*$^{PEK14\ \#10}$ (H), and Col-0 (J) pollen tubes. Pollen tubes measured in F, H, and J are indicated by white arrow heads in E, G, and I, respectively.

and excluded from the nucleus. 3D reconstructions of dividing root tip cells revealed that PEK14-GFP localized in a pattern resembling the cell-plate-adjacent end of the phragmoplast from early phragmoplast initiation until termination of cytokinesis (Figure S3; Movies 1 and 2) This closely correlates with the position of the plus ends of the phragmoplast microtubules (Otegui and Staehelin 2000).

Next, mature pollen and pollen tubes from adult plants were imaged. In mature pollen grains, no GFP signal could be detected (data not shown). In pollen tubes at 7 h post-pollination, both *pek14-1*$^{PEK14\ \#9}$ and *pek14-1*$^{PEK14\ \#10}$ showed an above-background GFP signal at the pollen tube tip, indicating that PEK14-GFP was expressed in growing pollen tubes and located diffusely at the pollen tube tip (Figures 3E,G and S4). Quantification of the GFP signal indicates that it is clearly distinguishable from the autofluorescence present in Col-0 pollen tubes (Figure 3I,J) and that it is most concentrated at the terminal 100–200 μm (Figure 3F,H).

3.5 | A Small Reduction of Pollen Viability Is Detected in *PEK14* Mutants

To investigate pollen viability in the mutants, pollen was fluorescently labeled with FDA and propidium iodide (PI) (Figure 4). In this assay, live pollen grains will fluoresce green based on the uptake of FDA, while dead pollen grains will fluoresce magenta, based on the penetration of PI and the exclusion of FDA (Figure 4A–F). A small but significant pollen viability defect was detected in both *pek14-1* and *pek14-2*. Pollen viability dropped from 88% in Col-0 to 78% and 79% in *pek14-1* and *pek14-2*, respectively. 89% of *pek14-1*$^{PEK14\ \#9}$ pollen grains were viable, while only 82% of *pek14-1*$^{PEK14\ \#10}$ were viable. *pek14-1*$^{PEK14\ \#9}$ viability was thus statistically identical to Col-0 pollen, while *pek14-1*$^{PEK14\ \#10}$ pollen was reduced in viability (Figure 4G). Because both lines complement the seed-set phenotype, this—together with the rather minor effect—suggests that pollen viability is not causal to the seed-set phenotype of *pek14* mutants.

3.6 | *pek14-1* Pollen Tubes Can Grow to Full Length In Vivo and Target Ovules but Show Elongation and Flexibility Defects When Grown Semi-In Vivo

The ability of pollen tubes to grow and target ovules for the release of sperm cells is a fundamental requirement of fertilization. Since sperm cells are not mobile on their own, they are dependent on the correct growth of the pollen tube cell to arrive at their destination. Random seed loss suggested that loss of PEK14 does not impair the ability of the pollen tube to grow the full distance to the base of the pistil. To further address whether all steps of the pollen tube's path, including ovary and ovule targeting, can be executed by *pek14-1* pollen, we imaged pollen tubes in vivo.

Aniline blue staining allows for the visualization of pollen tubes growing through the stigma and transmitting tract and arriving at the ovules (Figure 5). As shown in panels A and B, many *pek14-1* pollen tubes grow to the base of the transmitting tract with no observed defect. When ovules found near the base of the transmitting tract were examined, there was also evidence that pollen tubes were capable of ovule targeting and rupturing. The hazy white signal seen at the tip of each pollen tube suggested rupture of the tube and release of its content (indicated with white arrowhead) for Col-0 (Figure 5C) and *pek14-1* (Figure 5D). To distinguish the funiculus from a pollen tube targeting the ovule—structures that appear visually similar—unfertilized *male sterility-1* (*ms1*) ovules were also stained with aniline blue. This enabled clear visualization of the funiculus in the absence of pollen tubes, allowing for easier differentiation between the two (Figure 5E). Figure 5F shows a diagram of the ovule to assist in the interpretation of Figure 5C–E.

With no qualitative defect observed in vivo, we decided to take a closer look at the growth of the pollen tube itself. Timelapse imaging was performed on pollen tubes that were grown for 45 min from 5 h post-pollination (hpp) to 5:45 hpp. From this, the rate of pollen tube growth was calculated as described in Materials and Methods and graphed (Figure 5G). While Col-0 pollen tubes grew at an average rate of 1.5 μm/min, this rate was reduced to 1.2 μm/min in *pek14-1*. The average growth rate of *pek14-1*$^{PEK14\ \#9}$ was around 1.5 μm/min as in Col-0, suggesting that the loss of PEK14 has a small but significant effect on the pollen tube growth rate, at least under semi-in vivo conditions.

Aside from reaching the appropriate length, the direction of pollen tube growth, based on chemical signaling, is also crucial for successful fertilization. Live imaging of pollen tubes growing through female tissue in vivo is difficult (Mizuta et al. 2024). However, semi-in vivo pollen tube growth can be used to determine the straightness of pollen tubes as they grow. Straightness is here used as the measure of how much a pollen tube deviates from a straight line as it grows, as described

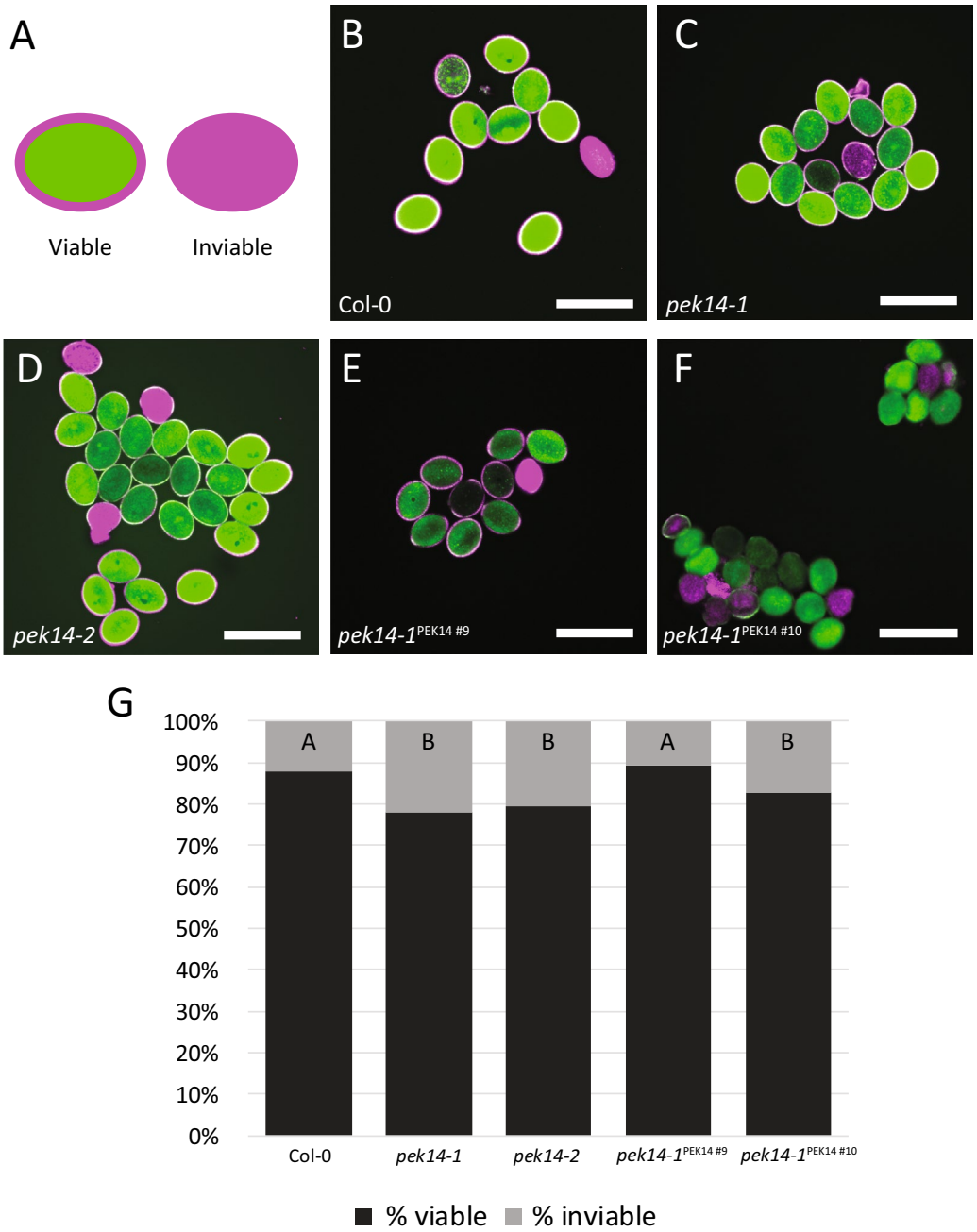

FIGURE 4 | Effect of *PEK14* mutations on pollen viability. (A) Cartoon diagram of dual viability staining with FDA (Green) and Propidium Iodide (Magenta). (B–F) Representative images of Col-0 (B), *pek14-1* (C), *pek14-2* (D), PEK14$_{pro}$::PEK14-GFP in *pek14-1* #9 (*pek14-1*$^{PEK14\ \#9}$) (E), and PEK14$_{pro}$::PEK14-GFP in *pek14-1* #10 (*pek14-1*$^{PEK14\ \#10}$) (F) pollen grains. Scale bars = 50 μm. (G) Quantification of viability stain. $N > 1000$ pollen grains for all lines. Statistical groups were created using a Fisher's Exact test and statistical group letters are indicated at the top of each column. Columns with the same letter are not significantly different.

in Materials and Methods. We measured the straightness of the terminal 100 μm from the pollen tube tip (Figure 5H). The straightness of *pek14-1* pollen tubes was 0.97, while that of Col-0 was 0.94, indicating that the mutant pollen tube tips bend and meander less during growth than those of Col-0. The straightness of *pek14-1*$^{PEK14\ \#9}$ pollen tubes was also examined and determined to be 0.94—identical to that of Col-0. Together, these data show that the loss of PEK14 leads to small but significant changes in both the growth rate and the pliability of the pollen tube tip.

3.7 | Trafficking of the Male Germ Unit Is Affected by the *PEK14* Mutation

Several studies have shown that the transport of the sperm cells together with the vegetative nucleus of the pollen are affected by MT depolymerization. In untreated pollen tubes, the vegetative nucleus (VN) and the two sperm cells (SCs) (together called the "male germ unit" or MGU) are closely connected and are found in close proximity to the pollen tube tip. After MT depolymerization, the distance to the tip increases and the VN and

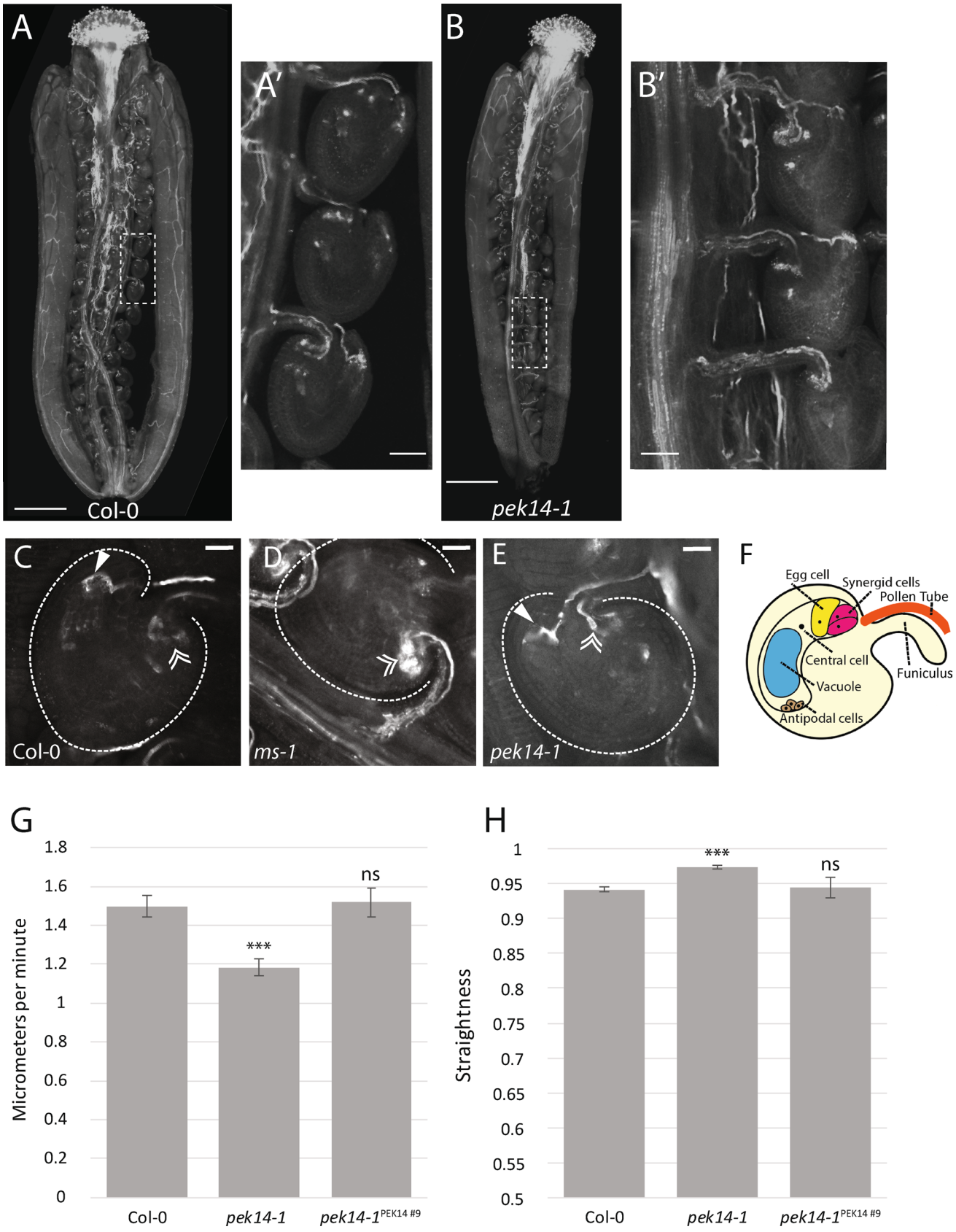

FIGURE 5 | Legend on next page.

SCs are less closely connected (Astrom et al. 1995; Laitiainen et al. 2002). Sometimes, they get trapped behind a callose plug, thus not reaching the pollen tube tip. The proximity of both the VN and SCs to the pollen tube tip is essential for robust fertilization (Zhou and Meier 2014; Zhang et al. 2017; Moser et al. 2020) and it has been proposed that kinesins could be involved in MGU

FIGURE 5 | *PEK14* mutant pollen tubes display defects in growth rate and straightness but can grow to full length and target ovules. (A–E) Aniline blue-stained pollen tubes growing into ovules in Col-0 and *pek14-1*. (A–B) Representative images of whole pistils. White dashed boxes indicate magnified areas shown in A′ and B′. Scale bar = 400 μm for A–B, and 50 μm for A′–B′. (C–D) Representative images showing pollen tube rupture at ovules. Aniline blue staining using pollen from (C) WT Col and (D) *pek14-1*. Solid arrow indicates site of pollen tube rupture. Double-chevron arrow indicates location of funiculus which also fluoresces after aniline blue staining. Scale bar = 20 μm. (E) Aniline blue staining of unpollinated *ms-1*. Double-chevron arrow indicates location of funiculus. Scale bar = 20 μm. (F) Diagram of ovule at same scale as (C–E). (G) The rate of pollen tube growth in μm per minute in a semi-in vivo pollen germination assay. $N > 40$ pollen tubes for all lines. Statistical analysis compared to Col-0 using Student's *t*-test: $p < 0.0005 = ***$. Error bars show standard error. (H) The straightness of Col-0, *pek14-1*, and $PEK14_{pro}$::PEK14-GFP in *pek14-1* #9 (*pek14-1*$^{PEK14\ \#9}$) pollen tube tips. $N > 40$ pollen tubes for all three lines. Statistical analysis compared to Col-0 using Student's *t*-test: $p < 0.0005 = ***$. Error bars show standard error.

transport during pollen tube growth (Schattner et al. 2021). Therefore, we investigated whether the distance of the MGU from the pollen tube tip and/or the connection of VN and SCs was altered in *pek14* mutants.

To visualize the MGU, pollen tubes were germinated and grown in the semi-in vivo system, stained with the nuclear stain SYBR green at 7 h post-pollination, and imaged as described in Materials and Methods. First, we categorized the order of the MGU, as several mutants with reduced male fertility show alterations in the normal appearance of VN ahead (closest to pollen tube tip), SCs following (Zhou and Meier 2014; Goto et al. 2020). The same alteration of order was also observed in MT depolymerization experiments (Heslop-Harrison and Heslop-Harrison 1997).

The MGU order was classified as belonging to one of the following categories: SC Ahead: The sperm cells were ahead of the VN, but not more than two lengths of the VN ahead of the VN. SC Far Ahead: The SCs were more than two VN lengths ahead of the VN. Overlapped: The SCs and VN were alongside one another. VN Only: Only the VN was visible within 100 μm of the pollen tube tip. VN Far Ahead: The VN was more than two lengths of the VN ahead of the SCs. VN Ahead: The VN was ahead of the SCs, but less than two lengths of the VN ahead of the SCs. Both *pek14-1* and *pek14-2* showed substantial defects in MGU order and VN-SC association (Figure 6A and Figure S5). The number of pollen tubes with an aberrant MGU order increased from 5% in Col-0 to 30% in *pek14-1* and 35% in *pek14-2*.

The most substantial aberrations were pollen tubes with only either the VN or the SCs present within the first 100 μm from the tip, followed by pollen tubes with SCs positioned ahead of the VN (Figures 6A and S5). *pek14-1*$^{PEK14\ \#9}$ and *pek14-1*$^{PEK14\ \#10}$ did not fully rescue the overall percentage of aberrant figures but notably eliminated the "VN only" and "SC only" categories and showed an increased amount of "overlapped" MGUs. This clearly indicates that the introduction of PEK14-GFP was sufficient to rescue the increased distancing between VN and SCs and thus the lost cohesion within the MGU.

We also investigated the distance of both VN and SCs from the pollen tube tip, using the measurements indicated in Figure 6B. Both VN and SCs were located significantly further from the pollen tube tip in *pek14-1* than in Col-0. Again, this defect was fully complemented by the expression of PEK14-GFP (Figure 6C).

4 | Discussion

Here, we have identified a role for the Arabidopsis kinesin-4 PEK14 (kinesin-4C) in male fertility, MGU organization, semi-in vivo pollen tube growth, and pollen tube tip straightness. PEK14 is the only Arabidopsis kinesin-4 expressed in pollen, but it is not specific for pollen. A second expression maximum is the meristematic zone of seedling roots, where we show the protein located at the growing rim of the cell plate, most likely through association within the phragmoplast midzone. However, we only observed phenotypes related to pollen, possibly because PEK14 is at least partially redundant to its family members kinesin-4A (FRA1) and kinesin-4C in roots and/or redundant to other kinesins.

FRA1 plays a role in the deposition of cellulose microfibrils (Zhong et al. 2002), while kinesin-4B has not yet been functionally investigated. FRA1 is needed for the development of proper cell wall strength, and loss of FRA1 can result in stunted plant growth due to a reduced ability of plant cells to undergo elongation (Kong et al. 2015; Zhu et al. 2015). FRA1 is localized at the cell periphery, where it assists in the trafficking and deposition of vesicles (Zhong et al. 2002; Kong et al. 2015; Zhu et al. 2015). This localization varies substantially from that of PEK14, which is located at the phragmoplasts of dividing root cells and the cytoplasm in non-dividing cells near the root apical meristem, as well as diffusely concentrated at the tips of pollen tubes.

Previous research demonstrated that a double mutant of *fra1* and *kinesin-4c* (*pek14-1*) displays a more severe *fra1* defect than *fra1* alone. This double mutant makes fewer seeds and is more stunted than *fra1* alone (Kong et al. 2015). It was proposed that this was the result of KINESIN-4C (PEK14) being functionally redundant to FRA1 in cell elongation in diverse plant tissues. However, no mutant phenotypes have been reported for *kinesin-4c* alone, and the enhanced fertility defects of the double mutant could be an indirect effect of the overall plant growth defects. Here, we show several specific defects of the *pek14-1* mutant pollen tubes that indicate a unique cellular role for this kinesin-4 in male fertility. All defects are relatively minor, suggesting that, again, PEK14 function in pollen might be redundant with other (in this case, non-kinesin-4) motor proteins. The defects include a small reduction in pollen viability, a small reduction in semi-in vivo pollen tube elongation, and a small decrease in meandering during pollen tube elongation. The most pronounced defect is a mis-organization of the MGU and an increase in its distance to the pollen tube tip. The PEK14-GFP fluorescent signal is diffusely detectable in pollen tubes with a concentration

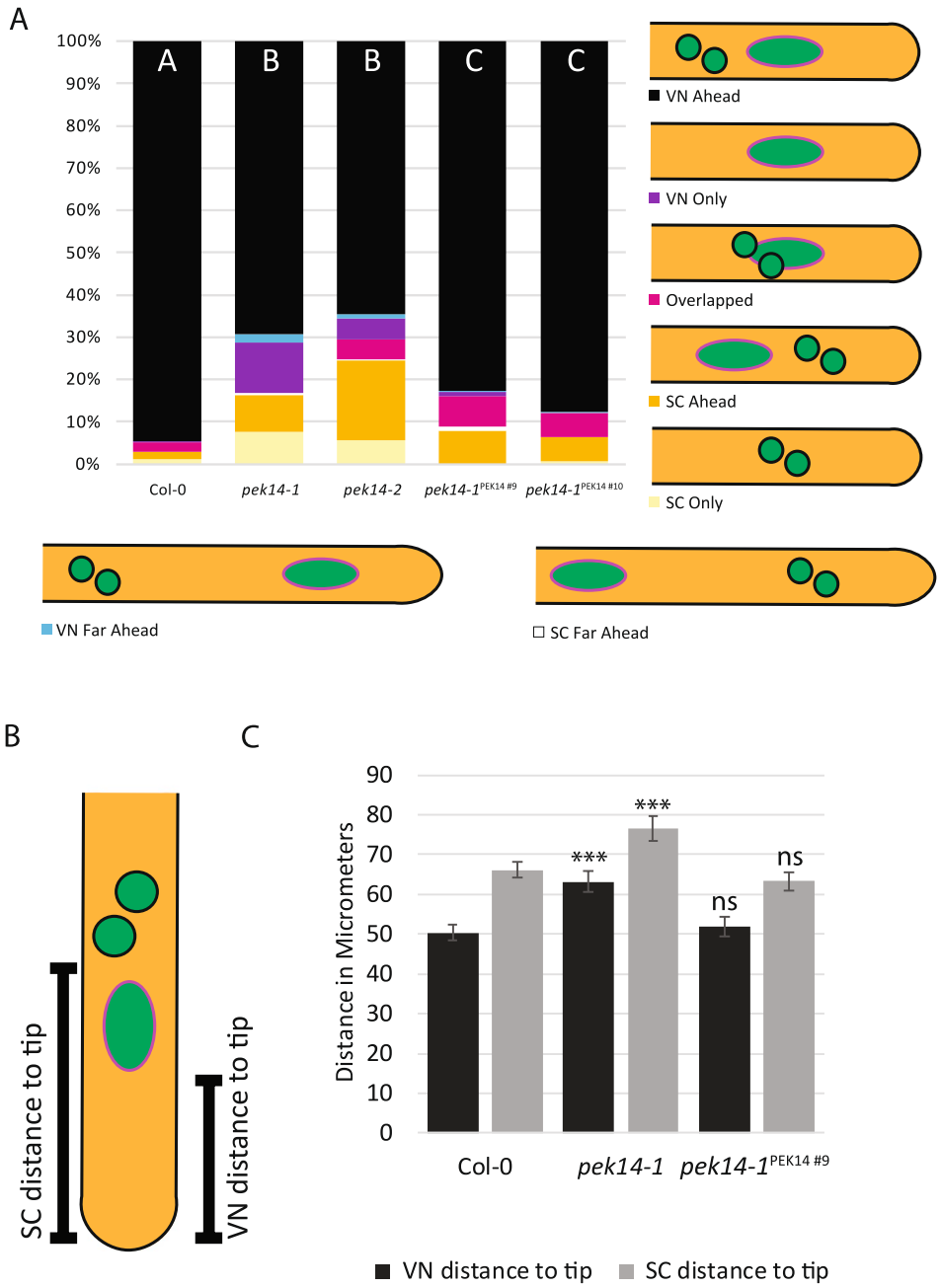

FIGURE 6 | The MGU order of PEK14 mutants is altered and has an increased distance to the pollen tube tip. (A) Order of the MGU in semi-in vivo germinated pollen tubes. Statistical groups were created using Fisher's Exact test and statistical group letters are indicated at the top of each column. Columns with the same letter are not significantly different. Diagrams for each classification of MGU order are shown, with the pollen tube growing to the right. $N > 100$ pollen tubes for each line. (B) Graphical representation of length measurements for VN distance to tip and SC distance to tip. (C) Distance of the leading edge of both the VN and the SCs to the pollen tube tip. $N > 30$ pollen tubes for all lines. Statistical analysis compared to Col-0 using Student's *t*-test: $P < 0.0005 = ***$. Error bars show standard error.

at the pollen tube tip, and its proposed roles have to take this localization into account.

PEK14 is the Arabidopsis kinesin most closely related to Pp-Kinesin04-Ia and Pp-Kinesin04-Ic of the moss *Physcomitrium patens* (Shen et al. 2012). These two kinesin-4 motors have been identified as necessary for proper antiparallel microtubule overlap at the phragmoplast during cell division. Despite the fundamental differences between plant and mammalian cytokinesis, this is similar to the function of human KIF4 at the MT overlaps of the midbody (Kurasawa et al. 2004; Zhu and Jiang 2005; Bieling et al. 2010). Pp-Kinesin04-Ia and Pp-Kinesin04-Ic line the tips of microtubules to delineate the length of microtubule overlap. Null mutants for Pp-Kinesin04-Ia and Pp-Kinesin04-Ic display a wider MT overlap and a thicker cell plate, which develops more slowly (de Keijzer et al. 2023). Additionally, when tip-growing moss caulonemal apical cells of *Δkin4-Ia* were examined, a defect in the growth pattern of these cells was observed. Instead of following a relatively sinuous path, *Δkin4-Ia* cells grew straighter with fewer deviations in growth direction

(de Keijzer et al. 2023). This, however, did not impact the growth rate. Rather, the growth direction was simply made more rigid—potentially reducing the colonies' ability to react to environmental signals (de Keijzer et al. 2023).

These phenotypes reported in moss are strikingly similar to the cellular phenotypes we have found for *pek14-1* in Arabidopsis pollen tubes—like moss caulonemal cells, a tip-growing cell type. Straightness analysis showed that, as in *Δkin4-Ia, pek14-1* pollen tubes become more straight in their growth pattern. However, pollen tube elongation is also only mildly affected. Additionally, like Pp-Kinesin04-Ia and Pp-Kinesin04-Ic, PEK14 is localized at the phragmoplast. Although the phragmoplast defect observed in *Δkin4-Ia* was not recapitulated in *pek14-1* root tip cells and no defect was observed in the growth of *pek14-1* roots (data not shown), this is possibly due to redundancy in the root. Together, this suggests that there is a conserved dual function of kinesin-4 motors in both moss and higher plants that combines an activity at the phragmoplast—possibly related to overlapping (+) ends like for human KIF4 (Hu et al. 2011)—with an activity modulating the elongation of tip-growing cells. It will be interesting in this context to investigate if PEK14 is also tip-localized in Arabidopsis elongating root hairs and if root hair elongation or stiffness shows similar defects as those observed for pollen tubes.

The role of microtubules and kinesins in the transport of the VN and the two SCs is still not well understood. Recently, it has been demonstrated that depolymerization of microtubules and inhibition of kinesin activity caused an increased velocity and greater amplitude in the saltatory movement of the VN and that microtubules are involved in coordinating the directional movement of the MGU. In contrast, inhibition of the actomyosin system did not cause a moving pattern change but influenced the overall velocity of the MGU. Based on these data, it was suggested that microtubules and kinesins play a role in avoiding the drifting of the MGU which would otherwise be caused by cytoplasmic streaming and the action of actin and myosin-based mobility (Wang et al. 2024). It is currently not known whether PEK14 is a motile kinesin and, if so, what the directionality of its movement is. If PEK14 is—in analogy to FRA1 and Pp-Kinesin04-Ia and Pp-Kinesin04-Ic—a (+) end-directed motor, then one possibility for how such an activity could influence MGU transport is by stabilizing a connection between the MGU and the pollen-tube tip. Instead of being associated with the MGU and providing movement along cortical MTs, as was suggested for MGU-moving motors by modeling (Schattner et al. 2021), PEK14, localized to the cell cortex or the actin cortical fringe, could exert force on microtubules that are stably associated with the surface of the MGU. If a class of VN-associated MTs had their minus ends at the pollen tube tip, PEK14 could then work in analogy to dynein on the astral microtubules during animal anaphase and exert a pulling motion on the VN. This would require a firm association of PEK14 in the tip region, likely through its cargo binding domain and currently unknown protein interaction partners.

Together, the cellular phenotypes of the *pek14-1* mutant described here, in conjunction with the localization pattern of PEK14, are informative to formulate further testable hypotheses towards a deeper understanding of the function of this formerly uncharacterized kinesin. One remaining riddle is how these phenotypes, which each are rather minor, together contribute to the relatively severe male-fertility phenotype. It is possible that this is caused by an additive effect of a series of small problems, each indicating an individual, likely at least semi-redundant function of PEK14. Alternatively, a currently still undiscovered additional role of PEK14 contributes in a more major way to the seed-loss phenotype.

Author Contributions

N.R.G. designed the study. I.M., N.R.G., and I.N.M. designed individual experiments, and I.N.M. performed most experiments. J.Z.L. and L.N.T. performed parts of the seed set and silique length screen. B.J.S. and A.Y.H. contributed the PEK14 cDNA. I.M., N.R.G., and I.N.M. wrote the manuscript. All authors proofread and edited the manuscript. I.M. provided oversight and funding.

Acknowledgments

We would like to thank all members of the Meier lab for fruitful discussions, particularly Ms. Katelyn Amstutz for critical reading and assistance with creating Figures 1A and S1.

Conflicts of Interest

The authors declare no conflicts of interest.

Data Availability Statement

The data that support the findings of this study are available on request from the corresponding author.

References

Aizawa, H., Y. Sekine, R. Takemura, Z. Zhang, M. Nangaku, and N. Hirokawa. 1992. "Kinesin Family in Murine Central Nervous System." *Journal of Cell Biology* 119, no. 5: 1287–1296. https://doi.org/10.1083/jcb.119.5.1287.

Alonso, J. M., A. N. Stepanova, T. J. Leisse, et al. 2003. "Genome-Wide Insertional Mutagenesis of Arabidopsis Thaliana." *Science* 301, no. 5633: 653–657. https://doi.org/10.1126/science.1086391.

Alvarez-Buylla, E. R., M. Benitez, A. Corvera-Poiré, et al. 2010. "Flower development." *Arabidopsis Book* 2010, no. 8: e0127. https://doi.org/10.1199/tab.0127.

Astrom, H., O. Sorri, and M. Raudaskoski. 1995. "Role of Microtubules in the Movement of the Vegetative Nucleus and Generative Cell in Tobacco Pollen Tubes." *Sexual Plant Reproduction* 8, no. 2: 61–69. https://doi.org/10.1007/bf00230890.

Avisar, D., M. Abu-Abied, E. Belausov, E. Sadot, C. Hawes, and I. A. Sparkes. 2009. "A Comparative Study of the Involvement of 17 Arabidopsis Myosin Family Members on the Motility of Golgi and Other Organelles." *Plant Physiology* 150, no. 2: 700–709. https://doi.org/10.1104/pp.109.136853.

Bannigan, A., W.-R. Scheible, W. Lukowitz, et al. 2007. "A Conserved Role for Kinesin-5 in Plant Mitosis." *Journal of Cell Science* 120, no. 16: 2819–2827. https://doi.org/10.1242/jcs.009506.

Bieling, P., I. A. Telley, and T. Surrey. 2010. "A Minimal Midzone Protein Module Controls Formation and Length of Antiparallel Microtubule Overlaps." *Cell* 142, no. 3: 420–432. https://doi.org/10.1016/j.cell.2010.06.033.

Cai, G. 2022. "The Legacy of Kinesins in the Pollen Tube 30 Years Later." *Cytoskeleton* 79, no. 1–3: 8–19. https://doi.org/10.1002/cm.21713.

Cai, G., and M. Cresti. 2010. "Microtubule Motors and Pollen Tube Growth—Still an Open Question." *Protoplasma* 247, no. 3: 131–143. https://doi.org/10.1007/s00709-010-0214-9.

Chebli, Y., J. Kroeger, and A. Geitmann. 2013. "Transport Logistics in Pollen Tubes." *Molecular Plant* 6, no. 4: 1037–1052. https://doi.org/10.1093/mp/sst073.

Clough, S. J., and A. F. Bent. 1998. "Floral Dip: A Simplified Method for *Agrobacterium*-Mediated Transformation of *Arabidopsis thaliana*." *Plant Journal* 16, no. 6: 735–743. https://doi.org/10.1046/j.1365-313x.1998.00343.x.

Day, R. C., S. Müller, and R. C. Macknight. 2009. "Identification of Cytoskeleton-Associated Genes Expressed During Arabidopsis Syncytial Endosperm Development." *Plant Signaling & Behavior* 4, no. 9: 883–886. https://doi.org/10.4161/psb.4.9.9461.

de Keijzer, J., R. van Spoordonk, J. E. van der Meer-Verweij, M. Janson, and T. Ketelaar. 2023. "Kinesin-4 Optimizes Microtubule Orientations for Responsive Tip Growth Guidance in Moss." *Journal of Cell Biology* 222, no. 9: e202202018. https://doi.org/10.1083/jcb.202202018.

Dickinson, H., J. Rodriguez-Enriquez, and R. Grant-Downton. 2018. "Pollen Germination and Pollen Tube Growth of Arabidopsis Thaliana: In Vitro and Semi In Vivo Methods." *Bio-Protocol* 8, no. 16: e2977. https://doi.org/10.21769/bioprotoc.2977.

Frey, N., J. Klotz, and P. Nick. 2010. "A Kinesin With Calponin-Homology Domain Is Involved in Premitotic Nuclear Migration." *Journal of Experimental Botany* 61, no. 12: 3423–3437. https://doi.org/10.1093/jxb/erq164.

Galindo-Trigo, S., T. M. Grand, C. A. Voigt, and L. M. Smith. 2020. "A Malectin Domain Kinesin Functions in Pollen and Seed Development in Arabidopsis." *Journal of Experimental Botany* 71, no. 6: 1828–1841. https://doi.org/10.1093/jxb/eraa023.

Ganguly, A., L. DeMott, and R. Dixit. 2017. "The Arabidopsis Kinesin-4, FRA1, Requires a High Level of Processive Motility to Function Correctly." *Journal of Cell Science* 130, no. 7: 1232–1238. https://doi.org/10.1242/jcs.196857.

Ganguly, A., C. Zhu, W. Chen, and R. Dixit. 2020. "FRA1 Kinesin Modulates the Lateral Stability of Cortical Microtubules Through Cellulose Synthase–Microtubule Uncoupling Proteins." *Plant Cell* 32, no. 8: 2508–2524. https://doi.org/10.1105/tpc.19.00700.

Gicking, A. M., K. W. Swentowsky, R. K. Dawe, and W. Qiu. 2018. "Functional Diversification of the Kinesin-14 Family in Land Plants." *FEBS Letters* 592, no. 12: 1918–1928. https://doi.org/10.1002/1873-3468.13094.

Goto, C., K. Tamura, S. Nishimaki, D. Maruyama, and I. Hara-Nishimura. 2020. "The Nuclear Envelope Protein KAKU4 Determines the Migration Order of the Vegetative Nucleus and Sperm Cells in Pollen Tubes." *Journal of Experimental Botany* 71, no. 20: 6273–6281. https://doi.org/10.1093/jxb/eraa367.

Haraguchi, T., K. Ito, Z. Duan, et al. 2018. "Functional Diversity of Class XI Myosins in *Arabidopsis thaliana*." *Plant & Cell Physiology* 59, no. 11: 2268–2277. https://doi.org/10.1093/pcp/pcy147.

Herrmann, A., P. Livanos, S. Zimmermann, et al. 2021. "KINESIN-12E Regulates Metaphase Spindle Flux and Helps Control Spindle Size in Arabidopsis." *Plant Cell* 33, no. 1: 27–43. https://doi.org/10.1093/plcell/koaa003.

Heslop-Harrison, J., and Y. Heslop-Harrison. 1997. "Microtubules and the Positioning of the Vegetative Nucleus and Generative Cell in the Angiosperm Pollen Tube: A Quantitative Study." *Proceedings of the Royal Society of London, Series B: Biological Sciences* 263, no. 1375: 1299–1304. https://doi.org/10.1098/rspb.1996.0190.

Hamilton, E. S., G. S. Jensen, G. Maksaev, A. Katims, A. M. Sherp, and E. S. Haswell. 2015. "Mechanosensitive channel MSL8 regulates osmotic forces during pollen hydration and germination." *Science* 350, no. 6259: 438–441. https://doi.org/10.1126/science.aac6014.

Hotta, T., Y.-R. J. Lee, T. Higaki, T. Hashimoto, and B. Liu. 2022. "Two Kinesin-14A Motors Oligomerize to Drive Poleward Microtubule Convergence for Acentrosomal Spindle Morphogenesis in Arabidopsis Thaliana." *Frontiers in Cell and Developmental Biology* 10: 949345. https://doi.org/10.3389/fcell.2022.949345.

Hu, C.-K., M. Coughlin, C. M. Field, and T. J. Mitchison. 2011. "KIF4 Regulates Midzone Length During Cytokinesis." *Current Biology* 21, no. 10: 815–824. https://doi.org/10.1016/j.cub.2011.04.019.

Jones, D. T., W. R. Taylor, and J. M. Thornton. 1992. "The Rapid Generation of Mutation Data Matrices From Protein Sequences." *Bioinformatics* 8, no. 3: 275–282. https://doi.org/10.1093/bioinformatics/8.3.275.

Kong, Z., M. Ioki, S. Braybrook, et al. 2015. "Kinesin-4 Functions in Vesicular Transport on Cortical Microtubules and Regulates Cell Wall Mechanics During Cell Elongation in Plants." *Molecular Plant* 8, no. 7: 1011–1023. https://doi.org/10.1016/j.molp.2015.01.004.

Kurasawa, Y., W. C. Earnshaw, Y. Mochizuki, N. Dohmae, and K. Todokoro. 2004. "Essential Roles of KIF4 and Its Binding Partner PRC1 in Organized Central Spindle Midzone Formation." *EMBO Journal* 23: 3237–3248. https://doi.org/10.1038/sj.emboj.7600347.

Laitiainen, E., K. M. Nieminen, H. Vihinen, and M. Raudaskoski. 2002. "Movement of Generative Cell and Vegetative Nucleus in Tobacco Pollen Tubes Is Dependent on Microtubule Cytoskeleton but Independent of the Synthesis of Callose Plugs." *Sexual Plant Reproduction* 15, no. 4: 195–204. https://doi.org/10.1007/s00497-002-0155-3.

Lawrence, C. J., R. K. Dawe, K. R. Christie, et al. 2004. "A Standardized Kinesin Nomenclature." *Journal of Cell Biology* 167, no. 1: 19–22. https://doi.org/10.1083/jcb.200408113.

Lebecq, A., A. Fangain, A. Boussaroque, and M.-C. Caillaud. 2022. "Dynamic Apico-Basal Enrichment of the F-Actin During Cytokinesis in Arabidopsis Cells Embedded in Their Tissues." *Quantitative Plant Biology* 3: e4. https://doi.org/10.1017/qpb.2022.1.

Lee, Y.-R. J., and B. Liu. 2004. "Cytoskeletal Motors in Arabidopsis. Sixty-One Kinesins and Seventeen Myosins." *Plant Physiology* 136, no. 4: 3877–3883. https://doi.org/10.1104/pp.104.052621.

Lipka, E., A. Gadeyne, D. Stöckle, et al. 2014. "The Phragmoplast-Orienting Kinesin-12 Class Proteins Translate the Positional Information of the Preprophase Band to Establish the Cortical Division Zone in *Arabidopsis thaliana*." *Plant Cell* 26, no. 6: 2617–2632. https://doi.org/10.1105/tpc.114.124933.

McElver, J., I. Tzafrir, G. Aux, et al. 2001. "Insertional Mutagenesis of Genes Required for Seed Development in *Arabidopsis thaliana*." *Genetics* 159, no. 4: 1751–1763. https://doi.org/10.1093/genetics/159.4.1751.

Meier, N. D., K. Seward, J. L. Caplan, and S. P. Dinesh-Kumar. 2023. "Calponin Homology Domain Containing Kinesin, KIS1, Regulates Chloroplast Stromule Formation and Immunity." *Science Advances* 9, no. 43: eadi7407. https://doi.org/10.1126/sciadv.adi7407.

Miki, H., M. Setou, K. Kaneshiro, and N. Hirokawa. 2001. "All Kinesin Superfamily Protein, KIF, Genes in Mouse and Human." *National Academy of Sciences of the United States of America* 98, no. 13: 7004–7011. https://doi.org/10.1073/pnas.111145398.

Mizuta, Y., D. Sakakibara, S. Nagahara, et al. 2024. "Deep Imaging Reveals Dynamics and Signaling in One-To-One Pollen Tube Guidance." *EMBO Reports* 25: 2529–2549. https://doi.org/10.1038/s44319-024-00151-4.

Mori, T., H. Kuroiwa, T. Higashiyama, and T. Kuroiwa. 2006. "GENERATIVE CELL SPECIFIC 1 Is Essential for Angiosperm Fertilization." *Nature Cell Biology* 8, no. 1: 64–71. https://doi.org/10.1038/ncb1345.

Moser, M., A. Kirkpatrick, N. R. Groves, and I. Meier. 2020. "LINC-Complex Mediated Positioning of the Vegetative Nucleus Is Involved in Calcium and ROS Signaling in Arabidopsis Pollen Tubes." *Nucleus* 11, no. 1: 149–163. https://doi.org/10.1080/19491034.2020.1783783.

Motomura, K., H. Takeuchi, M. Notaguchi, et al. 2021. "Persistent Directional Growth Capability in *Arabidopsis thaliana* Pollen Tubes After Nuclear Elimination From the Apex." *Nature Communications* 12, no. 1: 2331. https://doi.org/10.1038/s41467-021-22661-8.

Nebenführ, A., and R. Dixit. 2018. "Kinesins and Myosins: Molecular Motors That Coordinate Cellular Functions in Plants." *Annual Review of Plant Biology* 69: 329–361. https://doi.org/10.1146/annurev-arplant-042817-040024.

Otegui, M., and L. A. Staehelin. 2000. "Cytokinesis in Flowering Plants: More Than One Way to Divide a Cell." *Current Opinion in Plant Biology* 3, no. 6: 493–502. https://doi.org/10.1016/S1369-5266(00)00119-9.

Preuss, M. L., D. R. Kovar, Y.-R. J. Lee, C. J. Staiger, D. P. Delmer, and B. Liu. 2004. "A Plant-Specific Kinesin Binds to Actin Microfilaments and Interacts With Cortical Microtubules in Cotton Fibers." *Plant Physiology* 136, no. 4: 3945–3955. https://doi.org/10.1104/pp.104.052340.

Reddy, A. S., and I. S. Day. 2001. "Analysis of the Myosins Encoded in the Recently Completed Arabidopsis Thaliana Genome Sequence." *Genome Biology* 2, no. 7: RESEARCH0024.1. https://doi.org/10.1186/gb-2001-2-7-research0024.

Reddy, V. S., and A. S. N. Reddy. 2004. "Developmental and Cell-Specific Expression of ZWICHEL Is Regulated by the Intron and Exon Sequences of Its Upstream Protein-Coding Gene." *Plant Molecular Biology* 54, no. 2: 273–293. https://doi.org/10.1023/B:PLAN.0000028793.88757.8b.

Richardson, D. N., M. P. Simmons, and A. S. Reddy. 2006. "Comprehensive Comparative Analysis of Kinesins in Photosynthetic Eukaryotes." *BMC Genomics* 7, no. 1: 18. https://doi.org/10.1186/1471-2164-7-18.

Rigal, A., S. M. Doyle, and S. Robert. 2015. "Live Cell Imaging of FM4-64, a Tool for Tracing the Endocytic Pathways in Arabidopsis Root Cells." In *Plant Cell Expansion: Methods and Protocols. Methods and Protocols*, Methods in Molecular Biology, edited by J. M. Estevez. Humana Press. https://doi.org/10.1007/978-1-4939-1902-4.

Romagnoli, S., M. Cresti, and G. Cai. 2001. "Microtubule Motor Proteins and the Organization of the Pollen Tube Cytoplasm." *Sexual Plant Reproduction* 14, no. 1–2: 27–34. https://doi.org/10.1007/s004970100089.

Schattner, S., J. Schattner, F. Munder, E. Höppe, and W. J. Walter. 2021. "A Tug-Of-War Model Explains the Saltatory Sperm Cell Movement in Arabidopsis Thaliana Pollen Tubes by Kinesins With Calponin Homology Domain." *Frontiers in Plant Science* 11: 601282. https://doi.org/10.3389/fpls.2020.601282.

Schindelin, J., I. Arganda-Carreras, E. Frise, et al. 2012. "Fiji: An Open-Source Platform for Biological-Image Analysis." *Nature Methods* 9, no. 7: 676–682. https://doi.org/10.1038/nmeth.2019.

Sellers, J. R. 2000. "Myosins: A Diverse Superfamily." *Biochimica et Biophysica Acta* 1496, no. 1: 3–22. https://doi.org/10.1016/s0167-4889(00)00005-7.

Sessions, A., E. Burke, G. Presting, et al. 2002. "A High-Throughput Arabidopsis Reverse Genetics System." *Plant Cell* 14, no. 12: 2985–2994. https://doi.org/10.1105/tpc.004630.

Shen, Z., A. R. Collatos, J. P. Bibeau, F. Furt, and L. Vidali. 2012. "Phylogenetic Analysis of the Kinesin Superfamily From Physcomitrella." *Frontiers in Plant Science* 3: 230. https://doi.org/10.3389/fpls.2012.00230.

Shi, H., and R. A. Bressan. 2006. "RNA Extraction." In *Arabidopsis Protocols*, Methods in Molecular Biology, edited by J. Salinas and J. J. Sánchez-Serrano. Humana Press.

Sparkes, I. 2011. "Recent Advances in Understanding Plant Myosin Function: Life in the Fast Lane." *Molecular Plant* 4, no. 5: 805–812. https://doi.org/10.1093/mp/ssr063.

Spiegelman, Z., C.-M. Lee, and K. L. Gallagher. 2018. "KinG Is a Plant-Specific Kinesin That Regulates Both Intra- and Intercellular Movement of SHORT-ROOT." *Plant Physiology* 176, no. 1: 392–405. https://doi.org/10.1104/pp.17.01518.

Strauß, T., S. Schattner, S. Hoth, and W. J. Walter. 2021. "The Arabidopsis Thaliana Kinesin-5 AtKRP125b Is a Processive, Microtubule-Sliding Motor Protein With Putative Plant-Specific Functions." *International Journal of Molecular Sciences* 22, no. 21: 11361. https://doi.org/10.3390/ijms222111361.

Suetsugu, N., N. Yamada, T. Kagawa, et al. 2010. "Two Kinesin-Like Proteins Mediate Actin-Based Chloroplast Movement in Arabidopsis Thaliana." *Proceedings of the National Academy of Sciences of the United States of America* 107, no. 19: 8860–8865. https://doi.org/10.1073/pnas.0912773107.

Tamura, K., K. Nakatani, H. Mitsui, Y. Ohashi, and H. Takahashi. 1999. "Characterization of katD, a Kinesin-Like Protein Gene Specifically Expressed in Floral Tissues of Arabidopsis Thaliana." *Gene* 230, no. 1: 23–32. https://doi.org/10.1016/S0378-1119(99)00070-0.

Tamura, K., G. Stecher, and S. Kumar. 2021. "MEGA11: Molecular Evolutionary Genetics Analysis Version 11." *Molecular Biology and Evolution* 38, no. 7: 3022–3027. https://doi.org/10.1093/molbev/msab120.

Tiezzi, A., A. Moscatelli, G. Cai, A. Bartalesi, and M. Cresti. 1992. "An Immunoreactive Homolog of Mammalian Kinesin in Nicotiana Tabacum Pollen Tubes." *Cell Motility* 21, no. 2: 132–137. https://doi.org/10.1002/cm.970210206.

Vanstraelen, M., J. A. Torres Acosta, L. De Veylder, D. Inzé, and D. Geelen. 2004. "A Plant-Specific Subclass of C-Terminal Kinesins Contains a Conserved A-Type Cyclin-Dependent Kinase Site Implicated in Folding and Dimerization." *Plant Physiology* 135, no. 3: 1417–1429. https://doi.org/10.1104/pp.104.044818.

Vinogradova, M. V., G. G. Malanina, J. S. Waitzman, S. E. Rice, and R. J. Fletterick. 2013. "Plant Kinesin-Like Calmodulin Binding Protein Employs Its Regulatory Domain for Dimerization." *PLoS One* 8, no. 6: e66669. https://doi.org/10.1371/journal.pone.0066669.

Wang, S. Z., and R. Adler. 1995. "Chromokinesin: A DNA-Binding, Kinesin-Like Nuclear Protein." *Journal of Cell Biology* 128, no. 5: 761–768. https://doi.org/10.1083/jcb.128.5.761.

Wang, X., T. Li, J. Xu, et al. 2024. "Distinct Functions of Microtubules and Actin Filaments in the Transportation of the Male Germ Unit in Pollen." *Nature Communications* 15, no. 1: 5448. https://doi.org/10.1038/s41467-024-49323-9.

Wilson, Z. A., S. M. Morroll, J. Dawson, R. Swarup, and P. J. Tighe. 2001. "The Arabidopsis MALE STERILITY1 (MS1) Gene Is a Transcriptional Regulator of Male Gametogenesis, With Homology to the PHD-Finger Family of Transcription Factors." *Plant Journal* 28, no. 1: 27–39. https://doi.org/10.1046/j.1365-313X.2001.01125.x.

Winter, D., B. Vinegar, H. Nahal, R. Ammar, G. V. Wilson, and N. J. Provart. 2007. "An "Electronic Fluorescent Pictograph" Browser for Exploring and Analyzing Large-Scale Biological Data Sets." *PLoS One* 2, no. 8: e718. https://doi.org/10.1371/journal.pone.0000718.

Wu, S.-Z., and M. Bezanilla. 2014. "Myosin VIII Associates With Microtubule Ends and Together With Actin Plays a Role in Guiding Plant Cell Division." *eLife* 3: e03498. https://doi.org/10.7554/eLife.03498.

Yamada, M., Y. Tanaka-Takiguchi, M. Hayashi, M. Nishina, and G. Goshima. 2017. "Multiple Kinesin-14 Family Members Drive Microtubule Minus End–Directed Transport in Plant Cells." *Journal of Cell Biology* 216, no. 6: 1705–1714. https://doi.org/10.1083/jcb.201610065.

Yang, C., G. Vizcay-Barrena, K. Conner, and Z. A. Wilson. 2007. "MALE STERILITY1 Is Required for Tapetal Development and Pollen Wall Biosynthesis." *Plant Cell* 19, no. 11: 3530–3548. https://doi.org/10.1105/tpc.107.054981.

Yue, Y., T. L. Blasius, S. Zhang, et al. 2018. "Altered Chemomechanical Coupling Causes Impaired Motility of the Kinesin-4 Motors KIF27 and KIF7." *Journal of Cell Biology* 217, no. 4: 1319–1334. https://doi.org/10.1083/jcb.201708179.

Zhang, J., Q. Huang, S. Zhong, et al. 2017. "Sperm Cells Are Passive Cargo of the Pollen Tube in Plant Fertilization." *Nature Plants* 3: 17079. https://doi.org/10.1038/nplants.2017.79.

Zhong, R., D. H. Burk, W. H. Morrison III, and Z.-H. Ye. 2002. "A Kinesin-Like Protein Is Essential for Oriented Deposition of Cellulose Microfibrils and Cell Wall Strength." *Plant Cell* 14, no. 12: 3101–3117. https://doi.org/10.1105/tpc.005801.

Zhou, X., and I. Meier. 2014. "Efficient Plant Male Fertility Depends on Vegetative Nuclear Movement Mediated by Two Families of Plant Outer Nuclear Membrane Proteins." *Proceedings of the National Academy of Sciences of the United States of America* 111, no. 32: 11900–11905. https://doi.org/10.1073/pnas.1323104111.

Zhu, C., and R. Dixit. 2012. "Functions of the Arabidopsis Kinesin Superfamily of Microtubule-Based Motor Proteins." *Protoplasma* 249, no. 4: 887–899. https://doi.org/10.1007/s00709-011-0343-9.

Zhu, C., A. Ganguly, T. I. Baskin, et al. 2015. "The Fragile Fiber1 Kinesin Contributes to Cortical Microtubule-Mediated Trafficking of Cell Wall Components." *Plant Physiology* 167, no. 3: 780–792. https://doi.org/10.1104/pp.114.251462.

Zhu, C., and W. Jiang. 2005. "Cell Cycle-Dependent Translocation of PRC1 on the Spindle by Kif4 Is Essential for Midzone Formation and Cytokinesis." *Proceedings of the National Academy of Sciences of the United States of America* 102, no. 2: 343–348. https://doi.org/10.1073/pnas.0408438102.

Supporting Information

Additional supporting information can be found online in the Supporting Information section.